Available online at www.sciencedirect.com
ScienceDirect
Journal of Sound and Vibration 321 (2009) 220–241
JOURNAL OF SOUND AND VIBRATION
www.elsevier.com/locate/jsvi

Dynamic stability of thin-walled composite beams under periodic transverse excitation

Sebastián P. Machado[a,b,*], Víctor H. Cortínez[a,b]

[a]*Grupo Análisis de Sistemas Mecánicos, Facultad Regional Bahía Blanca, Universidad Tecnológica Nacional, 11de abril 461, B8000LMI Bahía Blanca, Argentina*
[b]*CONICET, Argentina*

Received 12 December 2007; received in revised form 18 July 2008; accepted 18 September 2008
Handling Editor: S. Bolton
Available online 31 October 2008

Abstract

The dynamic stability of thin-walled composite beams subjected to transverse external force has been investigated in this paper. The analysis is based on a seven-degree-of-freedom shear-deformable beam theory. A geometrically nonlinear theory is formulated in the context of large displacements and rotations. The regions of instability for simple and combination resonant frequencies are determined by applying Hsu's procedure to the Mathieu equation. This methodology is used for analyzing regions of dynamic instability of simply supported, cantilever and fixed-end beams considering open and closed cross-sections. The numerical results show the influence of the interaction between the forced vibration and the parametrically excited vibrations on the unstable regions size. Besides, the effect of geometrically nonlinear approximations is also analyzed. The analysis is supplemented by investigating the effects of the variation of load height parameter, beam length and fiber orientation angle.

1. Introduction

Composites are increasingly being used in the design of load-carrying members for the aerospace applications due to their outstanding engineering properties, such as high strength/stiffness to weight ratios and favorable fatigue characteristics. The interesting possibilities provided by fiber-reinforced composite materials can be used to enhance the response characteristics of such structures that operate in complex environmental conditions. As a result, a great amount of research has been devoted to study the static and dynamic responses of composites under different loading conditions.

On the other hand, structural collapse examples, such as the Tacoma Narrows Bridge in 1940 and the loss of dynamic stability of aircraft wings, showed that the instability issue should be considered in the structural design. Dynamic instability of elastic structural elements, such as rods, beams and columns, induced by parametric excitation has been investigated by many researchers. Extensive bibliographies on this subject were

*Corresponding author at: Grupo Análisis de Sistemas Mecánicos, Facultad Regional Bahía Blanca, Universidad Tecnológica Nacional, 11de abril 461, B8000LMI Bahía Blanca, Argentina. Tel.: +54 291 4555220; fax: +54 291 4555311.
E-mail addresses: smachado@frbb.utn.edu.ar (S.P. Machado), vcortine@frbb.utn.edu.ar (V.H. Cortínez).

0022-460X/$ - see front matter © 2008 Elsevier Ltd. All rights reserved.
doi:10.1016/j.jsv.2008.09.026

given by Evan-Iwanowski [1] and Nayfeh and Mook [2]. Bolotin [3] provided a general introduction to analyze the dynamic stability problems of various structural elements. The Mathieu–Hill equation is obtained in Refs. [1,3] while solving the parametric vibration of a beam subjected to a compressive dynamic force. Nayfeh and Mook [2], used the perturbation method to solve Mathieu–Hill's equation, in order to analyze the behavior of an elastic system under parametric excitation. They established a criterion to yield the transition curves by determining the characteristic exponents in the solution.

In relation to thin-walled beams, Gol'denblat [4] investigated the stability of a compressed thin-walled rod symmetrical about one axis. The problem was reduced to a system of two differential equations. Tso [5] studied the longitudinal–torsional stability, while Mettler [6] and Ghobarah and Tso [7] studied the bending–torsional stability of thin-walled beams. Bolotin [3,8] and Popelar [9,10] discussed the dynamic stability of thin-walled beams; typical I and H sections were considered. Hasan and Barr [11] evaluated regions of instability of thin-walled beams of equal angle-section, considering axial and transverse excitation in a cantilever beam. In spite of the practical interest and future potential of the thin-walled composite beam structures, particularly in the context of aerospace and mechanical applications, the main body of the available investigations has been devoted to the dynamic stability analysis of composite beams of solid sections [12,13].

On the other hand, the development of beam theories usually involves some type of reduction of the three-dimensional (3-D) constitutive relationships. Often this is accomplished by neglecting the stresses and strains in the transverse directions. For laminated composites, this is not necessarily an appropriate course of action. Bending–bending coupling caused by the Poisson effect, can be much greater in composite beams. Shear effect plays an important role in the behavior of linear [14–17] and nonlinear [18] stability of thin-walled composite beams, owing to the high ratio between the equivalent elasticity modulus and transverse elasticity modulus. To the best of author's knowledge, the dynamic stability analysis of a shear-deformable thin-walled composite beam was only presented by Machado and Cortínez [19]. They developed a second-order beam formulation to study the dynamic stability of beams subjected to axial external force. The Galerkin's method was used in order to discretize the governing equation and the Bolotin's method was applied to determine the regions of dynamic instability. The authors demonstrated that the size of the unstable regions can show a discrepancy depending on the influence of the longitudinal inertia.

In the present paper, this last work [19] is extended for the determination of dynamic instability regions of a thin-walled composite beam subjected to a transverse periodic excitation. It is necessary to extend the model because it is known that the classical and second-order beam theories underpredict and overpredict, respectively, the behavior of these structures [20,21]. Therefore, to avoid this difficulty it is necessary to consider a geometrically higher-order formulation. It should be emphasized here that the necessity of obtaining an accurate bending–torsional coupling arises from the fact that the stability behavior of this kind of structures is influenced by the initial displacements (corresponding to the static load) [20] and by the interaction between the forced vibration and the parametrically excited vibrations [19].

The purpose of the present investigation is the determination of the regions of dynamic instability of thin-walled composite beam subjected to a transverse periodic excitation, taking into account several non-classical effects. The analysis is based on a beam model formulated in the context of large displacements and rotations, through the adoption of a shear-deformable displacement field (accounting for bending and warping shear), considering a laminate stacking sequence symmetric and balanced. The numerical results are obtained for open and closed cross-section beam. The fiber orientation, the length beam and the load height parameter are varied to assess their effects on the dynamic instability behavior. The influence of shear deformation and inertial effects (corresponding to loading plane) on the unstable regions is analyzed. Ritz variational method is used to reduce the governing equation; the independent displacements vector is expressed as a linear combination of given x-function vectors and unknown t-function coefficients. Regions of dynamic instability of simple and combination resonances are determined by applying Hsu's [22] procedures to the Mathieu equation.

2. Kinematics

A straight thin-walled composite beam with an arbitrary cross-section is considered (Fig. 1). The points of the structural member are referred to a Cartesian coordinate system $(x, \bar{y}, \bar{z})$, where the x-axis is parallel to the

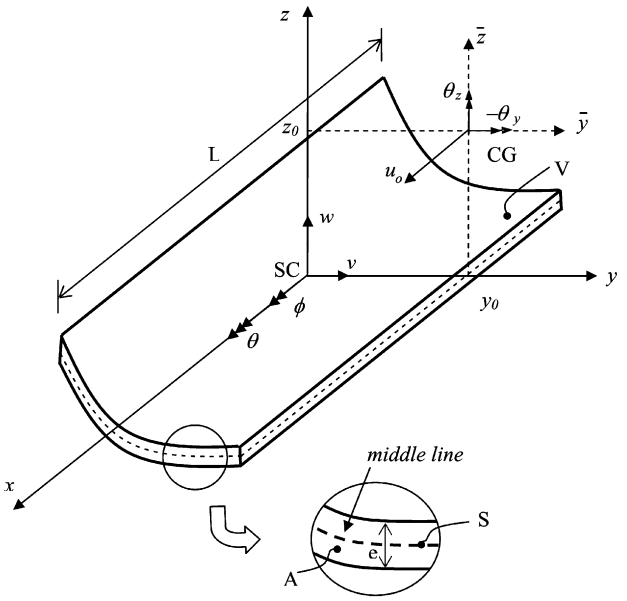

Fig. 1. Coordinate system of the cross-section and notation for displacement measures.

longitudinal axis of the beam while $\bar{y}$ and $\bar{z}$ are the principal axes of the cross-section. The axes y and z are parallel to the principal ones but having their origin at the shear center (defined according to Vlasov's theory of isotropic beams). The coordinates corresponding to points lying on the middle line are denoted as Y and Z (or $\bar{Y}$ and $\bar{Z}$). In addition, a circumferential coordinate s and a normal coordinate n are introduced on the middle contour of the cross-section

$$\bar{y}(s,n) = \bar{Y}(s) - n\frac{\mathrm{d}Z}{\mathrm{d}s}, \quad \bar{z}(s,n) = \bar{Z}(s) + n\frac{\mathrm{d}Y}{\mathrm{d}s}, \tag{1}$$

$$y(s,n) = Y(s) - n\frac{\mathrm{d}Z}{\mathrm{d}s}, \quad z(s,n) = Z(s) + n\frac{\mathrm{d}Y}{\mathrm{d}s}. \tag{2}$$

On the other hand, y_0 and z_0 are the centroidal coordinates measured with respect to the shear center

$$\begin{aligned} \bar{y}(s,n) &= y(s,n) - y_0, \\ \bar{z}(s,n) &= z(s,n) - z_0. \end{aligned} \tag{3}$$

The present structural model is based on the following assumptions:

(1) The cross-section contour is rigid in its own plane.
(2) The torsional warping distribution is assumed to be given by the Saint-Venant function for isotropic beams.
(3) Flexural rotations (about the $\bar{y}$ and $\bar{z}$ axes) are assumed to be moderate, while the twist ϕ of the cross-section can be arbitrarily large.
(4) Shell force and moment resultant corresponding to the circumferential stress σ_{ss} and the force resultant corresponding to γ_{ns} are neglected.
(5) The curvature at any point of the shell is neglected.
(6) Twisting linear curvature of the shell is expressed according to the classical plate theory.
(7) The laminate stacking sequence is assumed to be symmetric and balanced, or especially orthotropic [23,24].

According to the hypotheses of the present structural model, the displacement field proposed Eq. (4) is based on the principle of semi-tangential rotation defined by Argyris [25] to avoid the difficulty due to the

non-commutative nature of rotations. Besides, the nonlinear order of the terms corresponding to twist torsional is extended according to Hypothesis 3

$$\begin{aligned} u_x &= u_o - \bar{y}(\theta_z \cos\phi - \theta_y \sin\phi) - \bar{z}(\theta_y \cos\phi - \theta_z \sin\phi) + \omega\left[\theta - \tfrac{1}{2}(\theta'_y\theta_z - \theta_y\theta'_z)\right] \\ &\quad + (\theta_z z_0 - \theta_y y_0)\sin\phi, \\ u_y &= v - z\sin\phi - y(1-\cos\phi) - \tfrac{1}{2}\left(\theta_z^2\bar{y} + \theta_z\theta_y\bar{z}\right), \\ u_z &= w + y\sin\phi - z(1-\cos\phi) - \tfrac{1}{2}\left(\theta_y^2\bar{z} + \theta_z\theta_y\bar{y}\right). \end{aligned} \tag{4}$$

This expression is a generalization of others previously proposed in the literature as explained for Machado et al. [18]. The shear flexibility can be neglected considering $\theta_z = v'$, $\theta_y = w'$ and $\theta = \phi'$, to analyze its influence on the dynamic stability behavior. Moreover, the displacement field of the classical Vlasov theory is obtained when nonlinear effects are ignored. In the above expressions ϕ, θ_y and θ_z are measures of the rotations about the shear center axis, $\bar{y}$ and $\bar{z}$ axes, respectively. The variable θ is a measure of the torsional warping along the beam and in the present formulation is an independent variable [15]. Furthermore, the superscript 'prime' denotes derivation with respect to the variable x.

The warping function ω of the thin-walled cross-section may be defined as

$$\omega(s,n) = \omega_p(s) + \omega_s(s,n), \tag{5}$$

where ω_p and ω_s are the contour warping function and the thickness warping function, respectively. They are defined in the form [15,16,24]

$$\omega_p(s) = \frac{1}{S}\left[\int_0^S \left(\int_{s_0}^s [r(\sigma) - \psi(\sigma)]\,\mathrm{d}\sigma\right)\mathrm{d}s\right] - \int_{s_0}^s [r(\sigma) - \psi(\sigma)]\,\mathrm{d}\sigma,$$
$$\omega_s(s,n) = -nl(s), \tag{6a,b}$$

where σ is a dummy variable, and

$$r(s) = -Z(s)\frac{\mathrm{d}Y}{\mathrm{d}s} + Y(s)\frac{\mathrm{d}Z}{\mathrm{d}s}, \tag{7}$$

$$l(s) = Y(s)\frac{\mathrm{d}Y}{\mathrm{d}s} + Z(s)\frac{\mathrm{d}Z}{\mathrm{d}s}, \tag{8}$$

$r(s)$ represents the perpendicular distance from the shear center (SC) to the tangent at any point of the mid-surface contour and $l(s)$ represents the perpendicular distance from the shear center (SC) to the normal at any point of the mid-surface contour.

In Eq. (6a) Ψ is the shear strain at the middle line, obtained by means of the Saint-Venant theory of pure torsion for isotropic beams, and normalized with respect to $\mathrm{d}\phi/\mathrm{d}x$ [26]. For the case of open sections $\Psi = 0$.

3. The strain field

The displacements with respect to the curvilinear system (x, s, n) are obtained by means of the following expressions:

$$\bar{U} = u_x(x,s,n), \tag{9}$$

$$\bar{V} = u_y(x,s,n)\frac{\mathrm{d}Y}{\mathrm{d}s} + u_z(x,s,n)\frac{\mathrm{d}Z}{\mathrm{d}s}, \tag{10}$$

$$\bar{W} = -u_y(x,s,n)\frac{\mathrm{d}Z}{\mathrm{d}s} + u_z(x,s,n)\frac{\mathrm{d}Y}{\mathrm{d}s}. \tag{11}$$

The three non-zero components ε_{xx}, ε_{xs}, ε_{xn} of the Green's strain tensor are given by

$$\varepsilon_{xx} = \frac{\partial \overline{U}}{\partial x} + \frac{1}{2}\left[\left(\frac{\partial \overline{U}}{\partial x}\right)^2 + \left(\frac{\partial \overline{V}}{\partial x}\right)^2 + \left(\frac{\partial \overline{W}}{\partial x}\right)^2\right], \tag{12}$$

$$\varepsilon_{xs} = \frac{1}{2}\left[\frac{\partial \overline{U}}{\partial s} + \frac{\partial \overline{V}}{\partial x} + \frac{\partial \overline{U}}{\partial x}\frac{\partial \overline{U}}{\partial s} + \frac{\partial \overline{V}}{\partial x}\frac{\partial \overline{V}}{\partial s} + \frac{\partial \overline{W}}{\partial x}\frac{\partial \overline{W}}{\partial s}\right], \tag{13}$$

$$\varepsilon_{xn} = \frac{1}{2}\left[\frac{\partial \overline{U}}{\partial n} + \frac{\partial \overline{W}}{\partial x} + \frac{\partial \overline{U}}{\partial x}\frac{\partial \overline{U}}{\partial n} + \frac{\partial \overline{V}}{\partial x}\frac{\partial \overline{V}}{\partial n} + \frac{\partial \overline{W}}{\partial x}\frac{\partial \overline{W}}{\partial n}\right]. \tag{14}$$

Substituting Eq. (4) into Eqs. (9)–(11) and then into Eqs. (12)–(14), employing Eqs. (1)–(3) and Eqs. (5)–(8) after simplifying some higher-order terms, the components of the strain tensor are expressed in the following form:

$$\varepsilon_{xx} = \varepsilon_{xx}^{(0)} + n\kappa_{xx}^{(1)}, \quad \gamma_{xs} = 2\varepsilon_{xs} = \gamma_{xs}^{(0)} + n\kappa_{xs}^{(1)}, \quad \gamma_{xn} = 2\varepsilon_{xn} = \gamma_{xn}^{(0)}, \tag{15}$$

where

$$\begin{aligned}\varepsilon_{xx}^{(0)} = {} & u_o' + \frac{1}{2}\left(v'^2 + w'^2\right) + \omega_p\left[\theta' - \frac{1}{2}(\theta_z\theta_y'' - \theta_y\theta_z'')\right] + \overline{Z}(-\theta_y' \cos\phi + \theta_z' \sin\phi) \\ & + \overline{Y}(-\theta_z' \cos\phi - \theta_y' \sin\phi) + \frac{1}{2}\phi'^2(Y^2 + Z^2) + (z_0\theta_z' - y_0\theta_y')\sin\phi + \phi'(z_0\theta_z - y_0\theta_y)\cos\phi,\end{aligned} \tag{16}$$

$$\kappa_{xx}^{(1)} = -\frac{\mathrm{d}Z}{\mathrm{d}s}(-\theta_z' \cos\phi - \theta_y' \sin\phi) + \frac{\mathrm{d}Y}{\mathrm{d}s}(-\theta_y' \cos\phi + \theta_z' \sin\phi) - l\left[\theta' - \frac{1}{2}(\theta_z\theta_y'' - \theta_y\theta_z'')\right] - r\phi'^2, \tag{17}$$

$$\begin{aligned}\gamma_{xs}^{(0)} = {} & \frac{\mathrm{d}Y}{\mathrm{d}s}\left[(v' - \theta_z)\cos\phi - z_0\frac{1}{2}(\theta_z\theta_y' - \theta_y\theta_z') + (w' - \theta_y)\sin\phi\right] + (r - \psi)(\phi' - \theta) \\ & + \frac{\mathrm{d}Z}{\mathrm{d}s}\left[(w' - \theta_y)\cos\phi + y_0\frac{1}{2}(\theta_z\theta_y' - \theta_y\theta_z') - (v' - \theta_z)\sin\phi\right] + \psi\left[\phi' - \frac{1}{2}(\theta_z\theta_y' - \theta_y\theta_z')\right],\end{aligned} \tag{18}$$

$$\kappa_{xs}^{(1)} = -2\left[\phi' - \frac{1}{2}(\theta_z\theta_y' - \theta_y\theta_z')\right], \tag{19}$$

$$\begin{aligned}\gamma_{xn}^{(0)} = {} & \frac{\mathrm{d}Y}{\mathrm{d}s}\left[(w' - \theta_y)\cos\phi + y_0\frac{1}{2}(\theta_z\theta_y' - \theta_y\theta_z') - (v' - \theta_z)\sin\phi\right] \\ & - \frac{\mathrm{d}Z}{\mathrm{d}s}\left[(v' - \theta_z)\cos\phi - z_0\frac{1}{2}(\theta_z\theta_y' - \theta_y\theta_z') + (w' - \theta_y)\sin\phi\right] + l(\phi' - \theta).\end{aligned} \tag{20}$$

4. Variational formulation

Taking into account the adopted assumptions, the principle of virtual work for a composite shell may be expressed in the form [15,16,27]

$$\begin{aligned}& \iint\left(N_{xx}\delta\varepsilon_{xx}^{(0)} + M_{xx}\delta\kappa_{xx}^{(1)} + N_{xs}\delta\gamma_{xs}^{(0)} + M_{xs}\delta\kappa_{xs}^{(1)} + N_{xn}\delta\gamma_{xn}^{(0)}\right)\mathrm{d}s\,\mathrm{d}x \\ & - \iiint\rho\left(\ddot{u}_x\delta u_x + \ddot{u}_y\delta u_y + \ddot{u}_z\delta u_z\right)\mathrm{d}s\,\mathrm{d}n\,\mathrm{d}x - \iint(\bar{q}_z\delta\bar{u}_z)\,\mathrm{d}s\,\mathrm{d}x \\ & - \iint(\bar{p}_x\delta u_x)\big|_{x=0}\,\mathrm{d}s\,\mathrm{d}n - \iint(\bar{p}_x\delta u_x)\big|_{x=L}\,\mathrm{d}s\,\mathrm{d}n = 0,\end{aligned} \tag{21}$$

where N_{xx}, N_{xs}, M_{xx}, M_{xs} and N_{xn} are the shell stress resultants defined according to the following expressions:

$$N_{xx}=\int_{-e/2}^{e/2}\sigma_{xx}\,\mathrm{d}n,\quad M_{xx}=\int_{-e/2}^{e/2}(\sigma_{xx}n)\,\mathrm{d}n,$$
$$N_{xs}=\int_{-e/2}^{e/2}\sigma_{xs}\,\mathrm{d}n,\quad M_{xs}=\int_{-e/2}^{e/2}(\sigma_{xs}n)\,\mathrm{d}n,\quad N_{xn}=\int_{-e/2}^{e/2}\sigma_{xn}\,\mathrm{d}n. \tag{22}$$

The beam can be subjected to a wall surface traction $\bar{q}_z$ (specified per unit area of the undeformed middle surface and acting along the z-directions [18]) or to end traction $\bar{p}_x$ per unit area of the undeformed cross-section specified at $x=0$ and L, where L is the undeformed length of the beam [18]. Finally, $\bar{u}_z$ represent the vertical displacement at the middle line.

5. Constitutive equations

The constitutive equations of symmetrically balanced laminates may be expressed in the terms of shell stress resultants in the following form [23]:

$$\begin{Bmatrix} N_{xx}\\ N_{xs}\\ N_{xn}\\ M_{xx}\\ M_{xs}\end{Bmatrix}=\begin{bmatrix} \bar{A}_{11} & 0 & 0 & 0 & 0\\ 0 & \bar{A}_{66} & 0 & 0 & 0\\ 0 & 0 & \bar{A}_{55}^{(H)} & 0 & 0\\ 0 & 0 & 0 & \bar{D}_{11} & 0\\ 0 & 0 & 0 & 0 & \bar{D}_{66}\end{bmatrix}\begin{Bmatrix} \varepsilon_{xx}^{(0)}\\ \gamma_{xs}^{(0)}\\ \gamma_{xn}^{(0)}\\ \kappa_{xx}^{(1)}\\ \kappa_{xs}^{(1)}\end{Bmatrix} \tag{23}$$

with

$$\bar{A}_{11}=A_{11}-\frac{A_{12}^2}{A_{22}},\quad \bar{A}_{66}=A_{66}-\frac{A_{26}^2}{A_{22}},\quad \bar{A}_{55}^{(H)}=A_{55}^{(H)}-\frac{\left(A_{45}^{(H)}\right)^2}{A_{44}^{(H)}},$$
$$\bar{D}_{11}=D_{11}-\frac{D_{12}^2}{D_{22}},\quad \bar{D}_{66}=D_{66}-\frac{D_{26}^2}{D_{22}}, \tag{24}$$

where A_{ij}, D_{ij} and $A_{ij}^{(H)}$ are plate stiffness coefficients defined according to the lamination theory presented by Barbero [23]. The coefficient $\bar{D}_{16}$ has been neglected because of its low value for the considered laminate stacking sequence [15,16].

6. Principle of virtual work for thin-walled beams

Substituting Eqs. (16)–(20) into Eq. (21) and integrating with respect to s, one obtains the 1-D expression for the virtual work equation given by

$$L_M+L_K+L_P=0, \tag{25}$$

where L_M, L_K and L_P represent the virtual work contributions due to the inertial, internal and external forces, respectively. Their expressions are given below

$$L_M=\int_0^L\rho\Bigg[A\frac{\partial^2u_0}{\partial t^2}\delta u_0+I_z\frac{\partial^2\theta_z}{\partial t^2}\delta\theta_z+I_y\frac{\partial^2\theta_y}{\partial t^2}\delta\theta_y+C_w\frac{\partial^2\theta}{\partial t^2}\delta\theta+A\frac{\partial^2}{\partial t^2}(v-z_0\phi)\delta v$$
$$+A\frac{\partial^2}{\partial t^2}(w+y_0\phi)\delta w+\frac{\partial^2}{\partial t^2}(-Az_0v+Ay_0w+I_s\phi)\delta\phi\Bigg]\mathrm{d}x, \tag{26}$$

where A is the cross-sectional area, I_z and I_y are the principal moments of inertia of the cross-section, C_w is the warping constant, I_s the polar moment with respect to the shear center and ρ the mean density

of the laminate

$$
\begin{aligned}
L_K = \int_0^L \Big\{ & \delta u_0' \Big[N + u_0' N - M_z(\theta_z' \cos\phi + \theta_y' \operatorname{sen}\phi) - M_y(\theta_y' \cos\phi + \theta_z' \operatorname{sen}\phi) - Q_y(\theta_z \cos\phi + \theta_y \operatorname{sen}\phi) \\
& - Q_z(\theta_y \cos\phi + \theta_z \operatorname{sen}\phi) \Big] + \delta v'(Q_y \cos\phi - Q_z \operatorname{sen}\phi + v'N) + \delta w'(Q_z \cos\phi + Q_y \operatorname{sen}\phi + w'N) \\
& + \delta\theta_z \Big[-Q_y(1+u_0')\cos\phi + Q_z(1+u_0')\operatorname{sen}\phi + \tfrac{1}{2}(Q_z y_0 - Q_y z_0)\theta_y' - \tfrac{1}{2}T_{sv}\theta_y' - \tfrac{1}{2}B\theta_y'' \Big] \\
& + \delta\theta_z' \Big[-M_z(1+u_0')\cos\phi + M_y(1+u_0')\operatorname{sen}\phi + Nz_0 \operatorname{sen}\phi + \tfrac{1}{2}(Q_y z_0 - Q_z y_0)\theta_y + \tfrac{1}{2}T_{sv}\theta_y + \theta_z' P_{zz} + \theta_y' P_{yz} \Big] \\
& + \delta\theta_y \Big[-Q_z(1+u_0')\cos\phi - Q_y(1+u_0')\operatorname{sen}\phi + \tfrac{1}{2}(Q_y z_0 - Q_z y_0)\theta_z' + \tfrac{1}{2}T_{sv}\theta_z' + \tfrac{1}{2}B\theta_z'' \Big] \\
& + \delta\theta_y' \Big[-M_y(1+u_0')\cos\phi - M_z(1+u_0')\operatorname{sen}\phi - Ny_0 \operatorname{sen}\phi + \tfrac{1}{2}(Q_z y_0 - Q_y z_0)\theta_z - \tfrac{1}{2}T_{sv}\theta_z + \theta_z' P_{yz} + \theta_y' P_{yy} \Big] \\
& + \delta\phi \Big[M_y \Big(\underline{(\theta_y' + \theta_y' u_0')\operatorname{sen}\phi} + (\theta_z' + \theta_z' u_0')\cos\phi \Big) + M_z \Big(\underline{(\theta_z' + \theta_z' u_0')\operatorname{sen}\phi} - (\theta_y' + \theta_y' u_0')\cos\phi \Big) \\
& + Q_y \Big(\underline{(\theta_y - w' + \theta_z u_0')\operatorname{sen}\phi} - (\theta_y - w' + \theta_y u_0')\cos\phi \Big) + N(z_0\theta_z' - y_0\theta_y')\cos\phi \\
& + Q_z \Big(\underline{(\theta_y - w' + \theta_y u_0')\operatorname{sen}\phi} + (\theta_z - v' + \theta_z u_0')\cos\phi \Big) \Big] + \delta\theta_z'' \tfrac{1}{2} B\theta_y - \delta\theta_y'' \tfrac{1}{2} B\theta_z \\
& + \delta\phi'[T_w + T_{sv} + B_1\phi'] + \delta\theta' B - \delta\theta T_w \Big\} \mathrm{d}x.
\end{aligned} \tag{27}
$$

In the present study, the work done by the transverse periodic loads in the vertical plane is written as

$$
L_P = \int_0^L \left[-q_z(t)\delta w + \delta\phi\phi e_z q_z(t) \right] \mathrm{d}x + \left| \delta\theta_y \bar{M}_y(t) \right|_{x=0}^{x=L}, \tag{28}
$$

where the distributed load $q_z(t) = q_{z0} + q_{zt}\cos\varpi t$, ϖ is the excitation radian frequency, $q_{z0} = \alpha q_{\mathrm{cr}}$, $q_{zt} = \beta q_{\mathrm{cr}}$, α is the static load factor, β is the dynamic load factor, q_{cr} is the buckling load and e_z denotes the eccentricity in z-direction of the applied loads measured from the shear center. In what follows this last one will be called load height parameter. In the same way, $\bar{M}_y(t) = M_0 + M_t \cos\varpi t$ is the bending moment applied in the beam ends. However, when a concentrated load $P(t)$ is applied to the beam at the position $(x = a)$, instead of a distributed load, the load $q_z(t)$ in the potential L_P Eq. (28) is written as

$$
q_z(t) = P(t)\Delta(x - a), \tag{29}
$$

where Δ is the Dirac function.

6.1. Beam forces

In the above expressions, the following 1-D beam forces, in terms of the shell forces, have been defined

$$
\begin{aligned}
N &= \int N_{xx}\,\mathrm{d}s, \quad M_Y = \int \left(N_{xx}\bar{Z} + M_{xx}\frac{\mathrm{d}Y}{\mathrm{d}s} \right) \mathrm{d}s, \quad M_Z = \int \left(N_{xx}\bar{Y} - M_{xx}\frac{\mathrm{d}Z}{\mathrm{d}s} \right) \mathrm{d}s, \\
Q_Z &= \int \left(N_{xs}\frac{\mathrm{d}Z}{\mathrm{d}s} + N_{xn}\frac{\mathrm{d}Y}{\mathrm{d}s} \right) \mathrm{d}s, \quad Q_Y = \int \left(N_{xs}\frac{\mathrm{d}Y}{\mathrm{d}s} - N_{xn}\frac{\mathrm{d}Z}{\mathrm{d}s} \right) \mathrm{d}s, \\
T_w &= \int (N_{xs}(r - \psi) + N_{xn}l)\,\mathrm{d}s, \quad B = \int (N_{xx}\omega_p - M_{xx}l)\,\mathrm{d}s, \\
T_{\mathrm{sv}} &= \int (N_{xs}\psi - 2M_{xs})\,\mathrm{d}s,
\end{aligned} \tag{30}
$$

where the integration is carried out over the entire length of the mid-line contour. N corresponds to the axial force, Q_y and Q_z to the shear forces, M_y and M_z to the bending moments about y and z axes, respectively, B to the bimoment, T_w to the flexural–torsional moment and T_{sv} to the Saint-Venant torsional moment.

In addition, four higher-order stress resultants have been defined as follows:

$$B_1 = \int [N_{xx}(Y^2 + Z^2) - 2M_{xx}r]\,\mathrm{d}s, \quad P_{yy} = \int \left[N_{xx}\bar{Z}^2 + 2M_{xx}\bar{Z}\frac{\mathrm{d}Y}{\mathrm{d}s}\right]\mathrm{d}s,$$
$$P_{zz} = \int \left[N_{xx}\bar{Y}^2 - 2M_{xx}\bar{Y}\frac{\mathrm{d}Z}{\mathrm{d}s}\right]\mathrm{d}s, \quad P_{yz} = \int \left[N_{xx}\bar{Y}\bar{Z} + M_{xx}\left(\bar{Y}\frac{\mathrm{d}Y}{\mathrm{d}s} - \bar{Z}\frac{\mathrm{d}Z}{\mathrm{d}s}\right)\right]\mathrm{d}s. \tag{31}$$

The relationships among the generalized beam forces and the generalized strains characterizing the behavior of the beam are obtained by substituting Eqs. (16)–(20) into Eq. (23), and the results into Eq. (25). This constitutive law can be expressed in terms of a beam stiffness matrix **D** as defined in Appendix A.

6.2. Reduced model

The equations of motion of a beam subjected to a transverse excitation are reduced according to the Ritz method. The first step is to obtain the linearized response in the loading plane: $\mathbf{v} = \{u, v, \theta_z, w, \theta_y, \phi, \theta\}^{\mathrm{T}} = \{0, 0, 0, w, \theta_y, 0, 0\}^{\mathrm{T}}$. This part consists of a term corresponding to the static loading $\mathbf{v}_0(x)$ and the other corresponding to the dynamic loading $\mathbf{v}_1(x)\cos(\varpi t)$:

$$\mathbf{v}(x,t) = \mathbf{v}_0(x) + \mathbf{v}_1(x)\cos(\varpi t), \tag{32}$$

where it is assumed that $\mathbf{v}_1(x) \ll \mathbf{v}_0(x)$.

In order to analyze the dynamic stability of this motion, the flexural–torsional displacements $\mathbf{u} = \{0, v, \theta_z, 0, 0, \phi, \theta\}^{\mathrm{T}}$ are expressed as a linear combination of given x-function vectors $\mathbf{f}_k(x) = \{f_{k1}(x), f_{k2}(x), f_{k3}(x)\}$ and unknown t-function coefficients $q_k(t)$:

$$\mathbf{u}(x,t) = \sum_{k=1}^{n} q_k(t)\mathbf{f}_k(x). \tag{33}$$

The functions $\mathbf{f}_k(x)$ are chosen as eigenfunctions of the linearized equations and boundary conditions. In this case, the longitudinal displacement is decoupled from the rest and it is not considered. Now, introducing expressions corresponding to the loading plane equation (32) and flexural–torsional motion Eq. (33) into Eq. (25), taking variations with respect to the functions q_k and scaling the static load and dynamic amplitude with the critical buckling equivalent $M_0 = \alpha M_{\mathrm{cr}}$ and $M_t = \beta M_{\mathrm{cr}}$ (see Table 1), one can obtain Eq. (34)

$$\ddot{q}_k + \Omega_k^2 q_k + \beta M_{\mathrm{cr}}\eta\,\cos(\varpi t)\sum_{n=1}^{n} b_{kn}q_n = 0 \quad (k = 1, 2, \ldots, n), \tag{34}$$

where $(\Omega_k)^2$ are the system eigenvalues taking into account initial displacements due to the static load, βM_{cr} represents the excitation amplitude load, b_{kn} are the coefficients depending of the eigenfunctions, η is the coefficient that consider the interaction between the forced vibration and the parametrically excited vibrations on the unstable regions. It is important to remark that in Eq. (34) nonlinear terms associated with $\mathbf{v}_1(x)$ are neglected.

One should notice that the present formulation considers the inertial effects of the loading plane on the flexural–torsional vibrations. This influence is generally neglected in most of the dynamic instability studies. Such an assumption is valid to a certain extent when the exciting frequency is small in comparison with the frequency ω_p of the load plane free vibrations. This is the case frequently assumed for analyzing the dynamic stability of bars subjected to axial excitation [3,19,28]. However for transverse excitation, the frequency at which a parametric resonance occurs can be of the same order as the natural frequency of the loading plane vibrations. Therefore, in the present paper the contribution of the transverse vibration on the dynamic behavior is included.

The methodology explained above is illustrated for the case of simply supported beams subjected to uniform bending $\bar{M}_y(t) = M_0 + M_t\cos\varpi t$, where ϖ is the excitation frequency. In this case, the initial displacements are given by the following expressions:

$$w = \frac{M_0}{2\widehat{EI}_y}(Lx - x^2) + \frac{\widehat{GS}_z L\pi}{\widehat{GS}_z\pi^2 - L^2\rho A\varpi^2}\kappa_\theta M_t\,\cos(\varpi t)\sin(\pi x/L), \tag{35}$$

Table 1
Parameters in Eqs. (41)–(42)

Simply supported beam	C_1	C_2	β	δ
(a) End moments	1	0	0.5	0
(b) Uniformly distributed load ($M_{cr} = q_z L^2/8$)	1.141	0.459	0.033	0.214
(c) Concentrated force ($M_{cr} = PL/4$)	1.423	0.554	0.076	0.083

$$\theta_y = \frac{M_0}{2\widehat{EI}_y}(L-2x) + \kappa_\theta M_t \cos(\varpi t)\cos(\pi x/L), \tag{36}$$

where

$$\kappa_\theta = \frac{4L}{\widehat{EI}_y\pi^2 + L^2\left(\widehat{GS}_z - \rho I_y\varpi^2 + \widehat{GS}_z^2\pi^2\Big/\left(\varpi^2L^2\rho A - \pi^2\widehat{GS}_z\right)\right)}, \tag{37}$$

$\widehat{EI}_y$ is the flexural stiffness and $\widehat{GS}_z$ is the shear stiffness of a composite beam.

Therefore, the initial displacement expressions (w and θ_y) are composed of static and dynamic linear solution. Then, these last Eqs. (35)–(37) along with Eq. (33) are substituted into Eq. (25). So the resultant expression can be transformed to the following n coupled Mathieu equations Eq. (34). In this example, η has the following expression:

$$\eta = \frac{\widehat{EI}_y\pi^2}{\widehat{EI}_y\pi^2 + L^2\left(\widehat{GS}_z - \rho I_y\varpi^2 + \widehat{GS}_z^2\pi^2\Big/\left(\varpi^2L^2\rho A - \pi^2\widehat{GS}_z\right)\right)}. \tag{38}$$

When the influence of the interaction between the forced vibration and the parametrically excited vibrations is disregarded $\eta = 1$, which is obtained setting $\varpi = 0$ in Eq. (38).

7. Regions of instability

The different types of unstable boundaries for thin-walled composite beams subjected to transverse periodic load are studied in this section. The regions of instability for simple and combination resonant frequencies of sum type are determinate by applying Hsu's [22] procedures to the Mathieu equation (34). The method combines the method of variation of parameters and the series expansion of the perturbation method into a single treatment. The behavior of the non-trivial solutions in both the stable and unstable cases is deduced with the present analysis. The boundaries of the unstable regions are given as follows:

(a) *Simple resonance*, $\varpi = 2\Omega_k$:

$$2\Omega_k + \frac{\beta\eta b_{kk}}{2\Omega_k} > \varpi > 2\Omega_k - \frac{\beta\eta b_{kk}}{2\Omega_k}, \quad k = 1,2,\ldots,N. \tag{39}$$

(b) *Combination resonance of sum type*, $\varpi = \Omega_k + \Omega_j$:

$$(\Omega_k+\Omega_j) - \frac{\beta}{2}\eta\left(\frac{b_{kj}b_{jk}}{\Omega_k\Omega_j}\right)^{1/2} < \varpi < (\Omega_k+\Omega_j) + \frac{\beta}{2}\eta\left(\frac{b_{kj}b_{jk}}{\Omega_k\Omega_j}\right)1/2, \quad k\neq j, \quad k=j=1,2,\ldots,N. \tag{40}$$

8. Applications and numerical results

The purpose of this section is to apply the present theoretical model in order to study the dynamic stability of simply supported, cantilever and fixed-end thin-walled composite beams, considering open or closed bisymmetric cross-sections. The influence of shear deformation and geometrical nonlinear coupling is

analyzed for both simple and combination resonance. In this case, the transverse motion (w and θ_y) interacts with flexural–torsional motions (v, θ_z, ϕ and θ) as was explained in Section 6. In all the results presented below, the value of the static load parameter is adopted $\alpha = 0.5$, and the excitation frequency ϖ is scaled with the lowest frequency value of parametric resonance (that is the double of the frequency value of the vibration mode first $2\Omega_1$).

8.1. Bisymmetric open section subjected to uniform moments

The first example considered is a simply supported I-beam subjected to uniform bending moment $\bar{M}_y(t) = M_0 + M_t \cos \varpi t$ applied about its major axis. The geometrical properties are $h = 0.6\,\text{m}$, $b = 0.3\,\text{m}$, $e = 0.03\,\text{m}$, $L = 6\,\text{m}$ and the analyzed material is graphite-epoxy (AS4/3501) whose properties are $E_1 = 144\,\text{GPa}$, $E_2 = 9.65\,\text{GPa}$, $G_{12} = 4.14\,\text{GPa}$, $G_{13} = 4.14\,\text{GPa}$, $G_{23} = 3.45\,\text{GPa}$, $v_{12} = 0.3$, $v_{13} = 0.3$, $v_{23} = 0.5$, $\rho = 1389\,\text{kg/m}^3$. The influence of the interaction between the forced vibration and the parametrically excited vibrations is analyzed on the dynamic instability regions at twice frequencies $2\Omega_1$, $2\Omega_2$ and the combination frequency $\Omega_1 + \Omega_2$. Fig. 2 shows the dynamic stability behavior where the fiber orientation is varied to assess their effects on the instability regions.

The critical buckling load used to scale the static and dynamic load, $M_0 = \alpha M_{\text{cr}}$ and $M_t = \beta M_{\text{cr}}$, corresponding to the flexural–torsional mode, can be easily obtained by means of Eq. (41) (as explained by the authors in Ref. [20])

$$M_{\text{cr}} = C_1 \alpha \widehat{EI}_z \frac{\pi^2}{L^2}\left[-C_2 e_z \alpha + \sqrt{\frac{\widehat{GS}_w \widehat{GJ} + \widehat{EC}_w\left(\widehat{GS}_w + \widehat{GJ}\right)(\pi^2/L^2)}{\widehat{EI}_z(\pi^2/L^2)\left(\widehat{GS}_w + \widehat{EC}_w(\pi^2/L^2)\right)} + (C_2 e_z \alpha)^2}\right], \tag{41}$$

$$\alpha = \frac{1}{\sqrt{\left(1 - \frac{\widehat{EI}_z}{\widehat{EI}_y}\right)\left(1 - \beta\frac{\widehat{GJ}}{\widehat{EI}_y} - \beta\frac{\widehat{EC}_w \widehat{GS}_w \pi^2}{\widehat{EI}_y\left(\widehat{GS}_w L^2 + \widehat{EC}_w \pi^2\right)}\right) - \delta\frac{\widehat{EI}_z}{\widehat{GS}_y}\frac{\pi^2}{L^2}\left[1 - \frac{\widehat{GS}_y}{\widehat{GS}_z}\left(0.71 - \frac{\widehat{GS}_y}{\widehat{GS}_z}0.29\right)\right]}} \tag{42}$$

where C_1, C_2, β and δ are the approximate constants presented in Table 1. The critical values obtained by means of this formula take into account the effect of prebuckling deflections. On the other hand, natural frequencies values Ω_k (for $\beta = 0$) are obtained as explained in [21], taking into account the influence of the initial displacements.

The size of the principal unstable region (first mode) remains practically constant for the different sequences of lamination analyzed. While the second parametric (2° mode) and the combination resonance regions are influenced by the fibers orientation and by the effect of the in-plane loading inertia. The second parametric resonant region is higher for the lamination sequences $\{0/0/0/0\}$ and $\{0/90/90/0\}$ in comparison with the lamination $\{45/-45/-45/45\}$. This effect is partly due to the influence of the free vertical frequency ω_p, which is the same order as the parametric frequency $\varpi = 2\Omega_2$, for the two first laminations. While in the lamination $\{45/-45/-45/45\}$ the second parametric mode is more distant from the main unstable region. Therefore, the frequency ω_p is about the same order that the combination resonant frequency. The natural frequencies in Hz are shown in Table 2, for different sequences of lamination.

The influence of the interaction between the forced vibration and the parametrically excited vibrations on the unstable regions is analyzed in the figures. The unstable boundaries obtained by disregarding this interaction are drawn in dashed lines. The influence of this interaction enlarges the unstable region, which certainly is composed by two regions. Therefore, its discard results, inadvertently, in a less critical behavior than in the case of its incorporation.

On the other hand, to investigate the transverse shear effects, the results from the present theory are compared in terms of parametric resonance frequency with those obtained neglecting shear flexibility, for a lamination sequence $\{0/0/0/0\}$. The unstable regions of the first and second parametric resonance are shown in Figs. 3 and 4, where both models are compared. The width of the principal instability region is hardly the same for both models ($\Omega_1 = 21.23\,\text{Hz}$, without shear flexibility). However, neglecting shear flexibility, the free

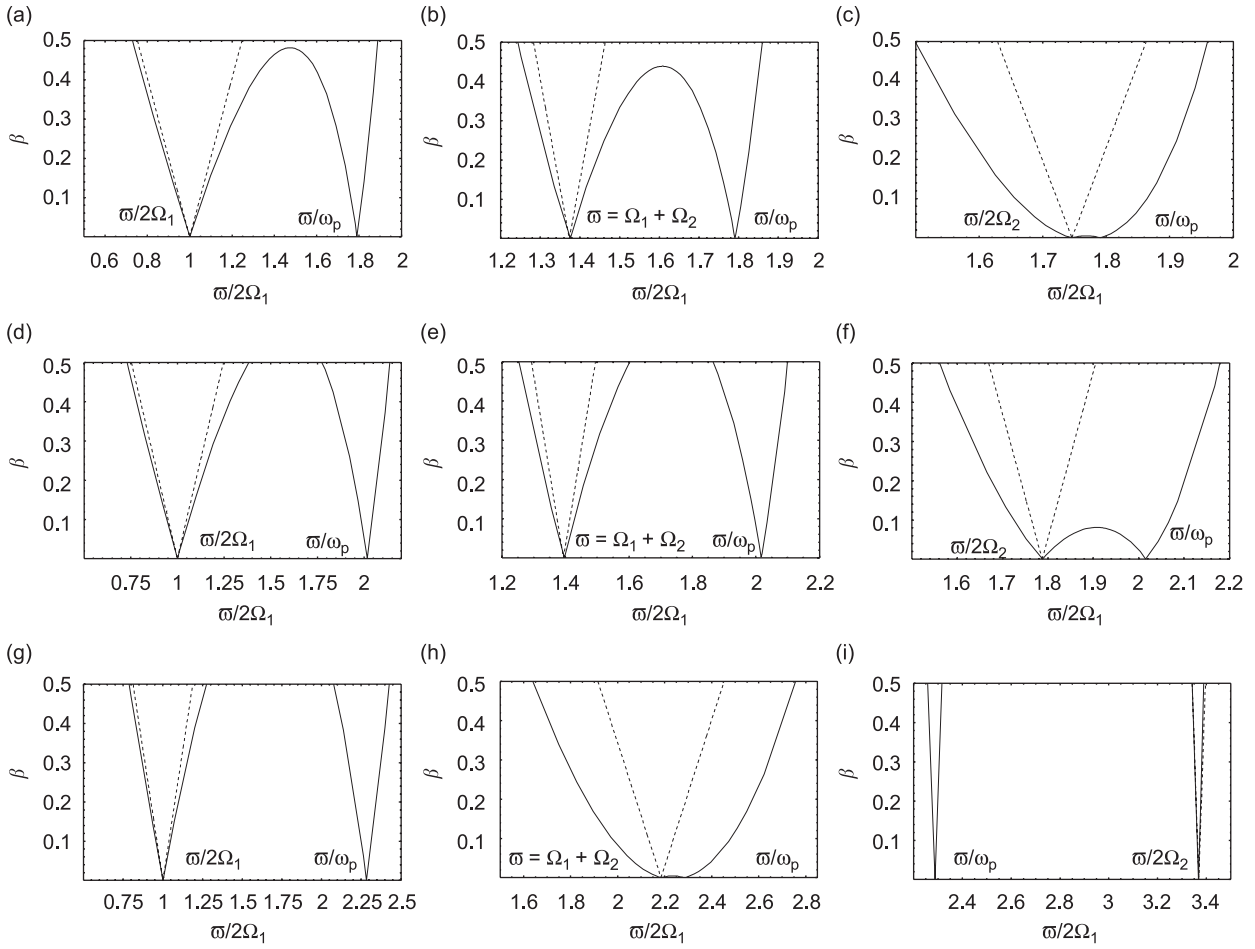

Fig. 2. Regions of dynamic instability, (——) present theory, (- - - - -) neglecting the influence of the transverse mode (loading plane), (a–c) correspond to a lamination sequence $\{0/0/0/0\}$, (d–f) to a lamination sequence $\{0/90/90/0\}$ and (g–i) to a lamination sequence $\{45/-45/-45/45\}$.

Table 2
Natural frequencies in Hz of a simply supported beam, $\beta = 0$

Lamination	Ω_1	Ω_2	ω_p
$\{0/0/0/0\}$	20.72	36.17	74.19
$\{0/90/90/0\}$	15.50	27.70	62.39
$\{45/-45/-45/45\}$	7.58	25.53	34.54

vertical frequency value is higher $\omega_p = 107.91$ Hz. Therefore, the effect of the interaction between both vibrations is worthless in the second parametric region (see Fig. 4) ($\Omega_2 = 37.72$ Hz, without shear flexibility).

8.2. Bisymmetric closed section subjected to a concentrated forced

In this example a simply supported box-beam loaded by a periodic force at the middle of the span is considered for two load positions. The load can be applied to the top (case a) or to the bottom beam face (case b). The geometrical properties are $h = 0.6$ m, $b = 0.3$ m, $e = 0.03$ m. The analyzed material is the same as

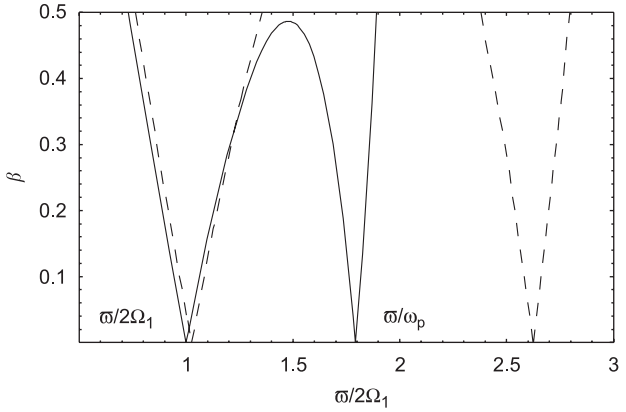

Fig. 3. Shear deformation influence on principal region of dynamic instability, considering interaction with ω_p, (———) present theory, (— — —) without shear deformation, for a lamination sequence $\{0/0/0/0\}$.

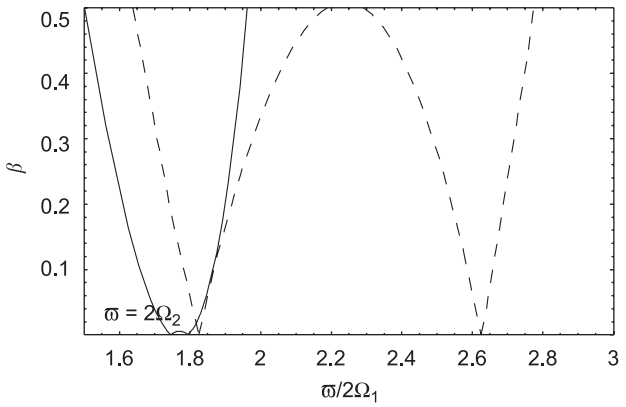

Fig. 4. Shear deformation influence on second parametric region of dynamic instability, considering interaction with ω_p, (———) present theory, (— — —) without shear deformation, for a lamination sequence $\{0/0/0/0\}$.

the previous examples graphite-epoxy, considering a lamination sequence $\{0/0/0/0\}$. In this section, the effect of the interaction between the forced vibration and the parametrically excited vibrations, the beam length, shear flexibility and height load parameter on the dynamic instability behavior of the composite beams is analyzed.

Figs. 5–8 show the unstable regions obtained by three different models: present formulation, neglecting shear flexibility and disregarding the interaction between the forced vibration and the parametrically excited vibrations, for two load positions and beam lengths, $L = 12$ and 6 m, respectively. The second parametric resonant frequency ($\varpi = 2\Omega_2$) is very large in comparison with the first parametric frequency when the length beam is $L = 12$ m. Therefore, the unstable region size is hardly insignificant and they are omitted in Figs. 5 and 7. Shear deformation effect has no influence in the size of the unstable regions. However, when this effect is neglected the regions of instability moves toward the right, originated by an increase in the parametric frequency values. In Table 3, buckling loads and natural frequencies values obtained with the present formulation and those obtained neglecting shear deformation are compared. The shear influence is more evident when the beam length decreases and this discrepancy can reach a percentage of about 30% for the natural frequency corresponding to the vertical plane ω_p. However, this effect remains constant when the load height is varied. On the other hand, the influence of interaction between forced vibration and the parametrically excited vibrations is more evident when the load is applied on top face. The principal instability regions without interaction are smaller than those obtained with the present theory, predicting a stable region

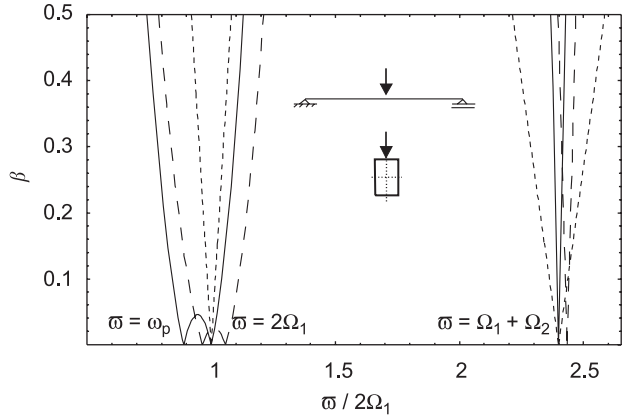

Fig. 5. Regions of dynamic instability, (———) present theory, (— — —) without shear deformation, (-----) neglecting interaction with ω_p, $e_z = h/2$, $L = 12\,\text{m}$.

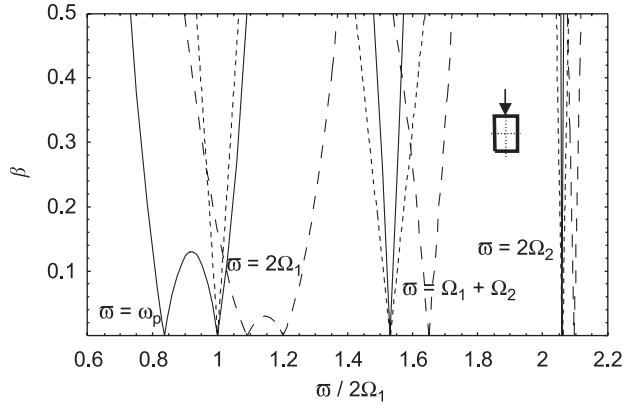

Fig. 6. Regions of dynamic instability, (———) present theory, (— — —) without shear deformation, (-----) neglecting interaction with ω_p, $e_z = h/2$, $L = 6\,\text{m}$.

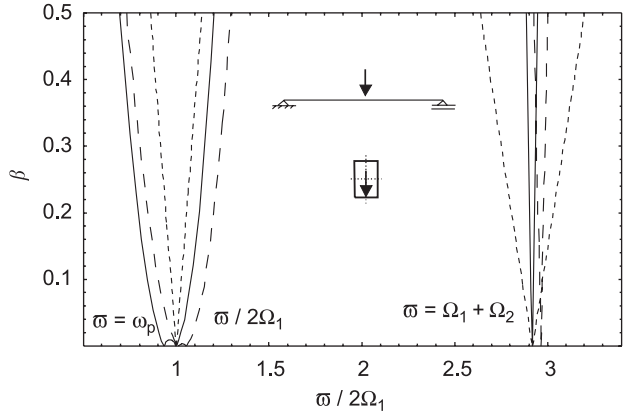

Fig. 7. Regions of dynamic instability, (———) present theory, (— — —) without shear deformation, (-----) neglecting interaction with ω_p, $e_z = -h/2$, $L = 12\,\text{m}$.

where in fact it is unstable. However, the second and third unstable regions, corresponding to combination and parametric resonant frequencies, are larger when the interaction is neglected, overpredicting the unstable behavior.

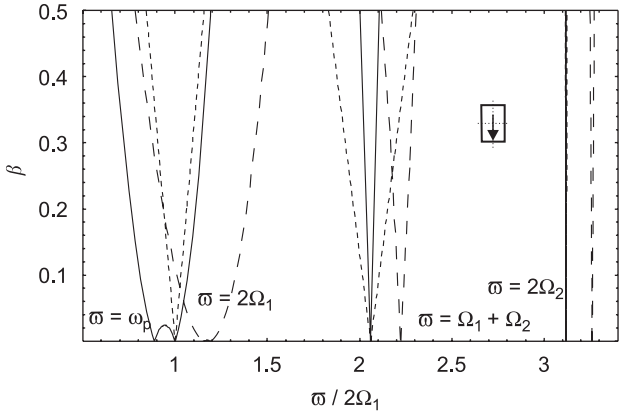

Fig. 8. Regions of dynamic instability, (———) present theory, (— — —) without shear deformation, (- - - - -) neglecting interaction with ω_p, $e_z = -h/2$, $L = 6\,\text{m}$.

Table 3
Shear effect on buckling load and natural frequencies values, for a simply supported box-section beam

Length (m)	Load height	Shear deformation	P_{cr} (MN)	Ω_1 (Hz)	Ω_2 (Hz)	ω_p (Hz)
12	Top	With	4.36	12.86	48.85	22.76
		Without	4.41	13.59	49.02	24.83
	Bottom	With	6.72	12.25	59.30	22.76
		Without	6.84	12.91	59.79	24.83
6	Top	With	13.95	45.03	93.27	75.68
		Without	14.44	54.01	94.95	98.67
	Bottom	With	31.41	41.57	133.28	75.68
		Without	33.89	49.27	139.34	98.67

8.3. Simply supported beam subjected to distributed load

In this example a simply supported beam under distributed load $qz(t) = qz_0 + qz_t \cos \varpi t$ is considered for three load positions. The load can be applied to the top flange (case a), at the shear center (case b), and to the bottom flange (case c). The beam considered is a bisymmetric-I section whose geometric properties are $h = 0.6\,\text{m}$, $b = 0.6\,\text{m}$, $e = 0.03\,\text{m}$, $L = 6\,\text{m}$. The analyzed material is the same as the previous examples. The buckling load used to scale the static load $qz_0 = \alpha q_{cr}$, corresponding to the flexural–torsional mode, can be easily obtained by means of Eq. (41) along with Table 1. On the other hand, as in the previous examples the natural frequencies values Ω_k (for $\beta = 0$) are obtained as explained by Machado and Cortínez in [21], taking into account initial displacements.

Instability regions are shown in Figs. 9–11, considering different load heights and for a sequence of lamination $\{0/0/0/0\}$. It is observed that the widest unstable region corresponds to the first mode (or to the first frequency of parametric resonance), while the smallest region correspond to the parametric excited second mode. The intermediate region is due to combination resonance of the two first modes. Comparative results between the unstable regions obtained by disregarding and considering the influence of the inertia in the loading plane are shown in the figures. In this case, the natural frequency corresponding to the loading plane ω_p is lower than the first parametric resonance frequency $2\Omega_1$. The influence of the vertical inertia enlarges the first region, which certainly is composed by two regions. For example, when the load is applied on the top flange (Fig. 9), one region lies near $\varpi = 2\Omega_1 = 81.87\,\text{Hz}$ and the other lies near $\varpi = \omega_p = 67.77\,\text{Hz}$, for $\beta = 0$. On the other hand, when the load is applied on the bottom flange (Fig. 11), the first unstable region is largest

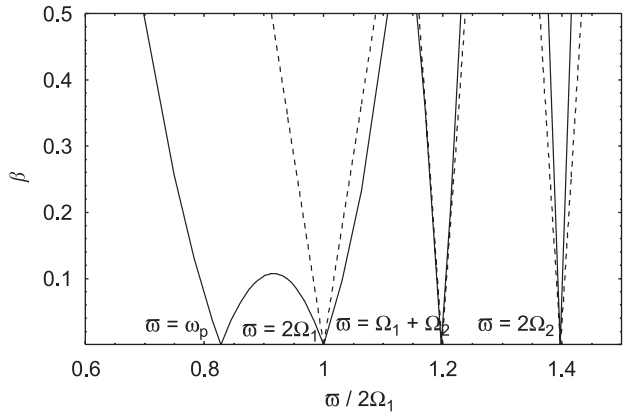

Fig. 9. Regions of dynamic instability for an excitation load applied in the top flange, (———) present theory, (- - - - -) neglecting interaction with ω_p, for a lamination sequence $\{0/0/0/0\}$.

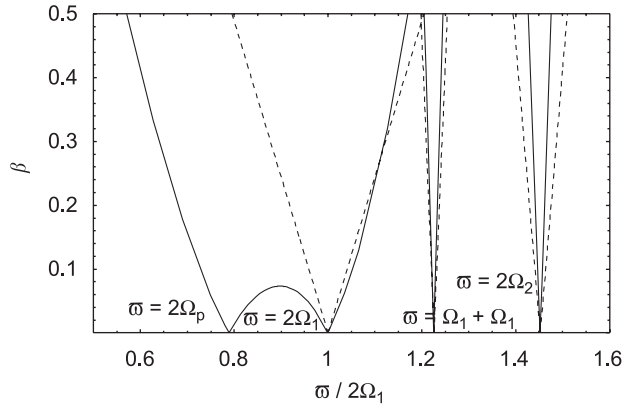

Fig. 10. Regions of dynamic instability for an excitation load applied in the shear center, (———) present theory, (- - - - -) neglecting interaction with ω_p, for a lamination sequence $\{0/0/0/0\}$.

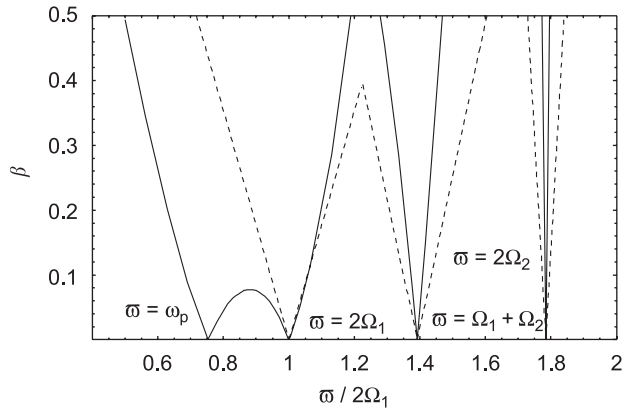

Fig. 11. Regions of dynamic instability for an excitation load applied in the bottom flange, (———) present theory, (- - - - -) neglecting interaction with ω_p, for a lamination sequence $\{0/0/0/0\}$.

in comparison with the other load condition (Figs. 9 and 10). However, the third region (second simple resonance mode) is smallest due to the parametric frequency ($\varpi = 2\Omega_2$) is more distant from the principal region.

A similar behavior is observed for a sequence of lamination $\{0/90/90/0\}$ in Figs. 12–14, considering the three load conditions. In this case, the loading plane frequency ω_p is hardly next to the first frequency excited

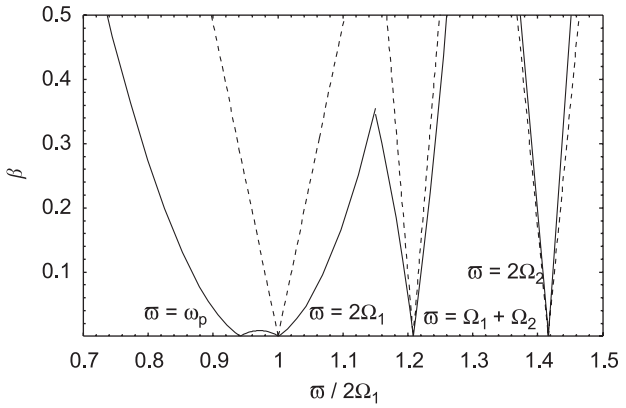

Fig. 12. Regions of dynamic instability for an excitation load applied in the top flange, (———) present theory, (- - - - -) neglecting interaction with ω_p, for a lamination sequence $\{0/90/90/0\}$.

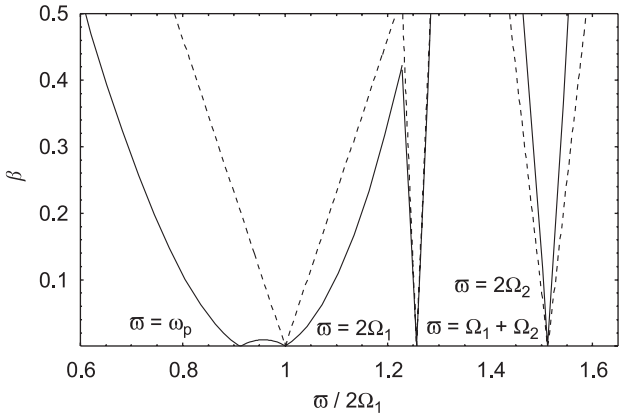

Fig. 13. Regions of dynamic instability for an excitation load applied in the shear center, (———) present theory, (- - - - -) neglecting interaction with ω_p, for a lamination sequence $\{0/90/90/0\}$.

parametrically ($2\Omega_1$). As the value of dynamical load parameter β increases, the main unstable region gets together with the combination resonance region ($\Omega_1+\Omega_2$). The size of the third unstable region ($\varpi = 2\Omega_2$) is almost insignificant when the load is applied on the bottom flange. The influence of the interaction between the forced vibration and the parametrically excited vibrations is significant in the three load conditions. When the interaction is ignored the main unstable regions are smaller and this effect is more notable when the fibers are oriented in the longitudinal direction. However, the third unstable regions are larger when this effect is neglected, overpredicting the unstable behavior.

8.4. Cantilever beam subjected to end force

The example considered is a cantilever beam subjected to end force applied in the shear center of its free end. The cross-section properties of the I-beam and the material properties are the same as the previous example, considering in this case a beam length of $L = 12$ m. Regions of dynamic instability for the composite beam are shown in Fig. 15, considering a lamination sequence $\{0/90/90/0\}$. The influence of the interaction between the forced vibration and the parametrically excited vibrations on the unstable regions is analyzed in the figure. The unstable boundaries obtained by disregarding this interaction are drawn in dashed lines. In this case, the natural frequency corresponding to the loading plane (ω_p) is hardly higher than the first parametric resonance frequency ($2\Omega_1$). The influence of the vertical inertia enlarges the instability region to high frequency values, until it merges with the combination resonance region. Therefore, it derives in a large region which certainly is composed by three regions, one of them corresponding to the principal unstable region ($2\Omega_1 = 6.94$ Hz), the

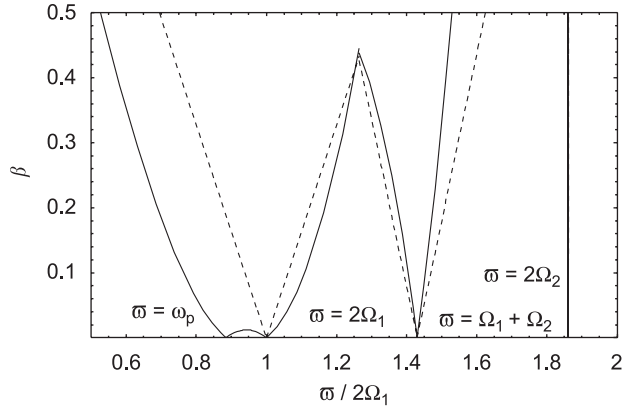

Fig. 14. Regions of dynamic instability for an excitation load applied in the bottom flange, (———) present theory, (- - - - -) neglecting interaction with ω_p, for a lamination sequence $\{0/90/90/0\}$.

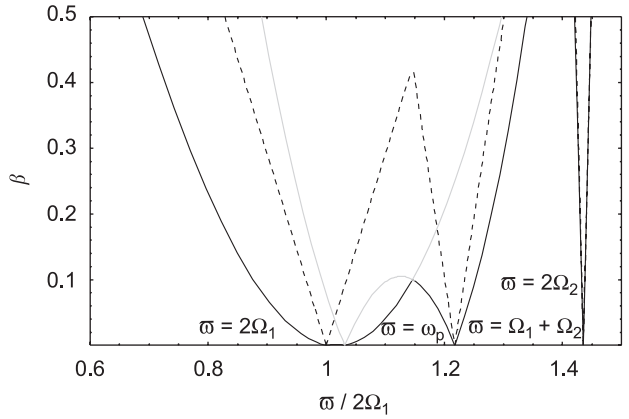

Fig. 15. Unstable regions of a cantilever beam, (———) present theory, (- - - - -) neglecting interaction with ω_p.

other corresponding to in-plane loading vibration mode ($\omega_p = 7.16\,\text{Hz}$), and the last one corresponding to the combination resonance region ($\Omega_1 + \Omega_2 = 8.45\,\text{Hz}$), for $\beta = 0$. The unstable regions are smaller when the interaction of the forced vibration is omitted, predicting a less critical behavior.

8.5. Fixed-end beam subjected to a concentrated force

In this example a fixed-end beam is excited transversely by a force at the middle of the span applied in the shear center. The length beam and the sequence of lamination are the same as the previous case, but the analyzed material is glass-epoxy whose properties are $E_1 = 48.3\,\text{GPa}$, $E_2 = 19.8\,\text{GPa}$, $G_{12} = 8.96\,\text{GPa}$, $G_{13} = 8.96\,\text{GPa}$, $G_{23} = 6.19\,\text{GPa}$, $v_{12} = 0.27$, $v_{13} = 0.27$, $v_{23} = 0.6$, $\rho = 1389\,\text{kg/m}^3$.

In Fig. 16, the regions of dynamic instability are shown for two values of the static load parameter, $\alpha = 0.1$ and 0.5. The vibration frequency values decrease as the static load factor increases. In this example, the natural frequency corresponding to the loading plane is $\omega_p = 28.96\,\text{Hz}$. For a small static load parameter ($\alpha = 0.1$), the influence of the vertical inertia enlarges the unstable region to low-frequency values. It is due to the main parametric frequency is larger ($2\Omega_1 = 33.24\,\text{Hz}$) than the free vertical frequency ω_p. Besides, it is observed from Fig. 16a, that the instability region is composed by four regions, one of them corresponding to loading in-plane vibration mode, two corresponding to the first and second parametric resonance and the last one corresponding to the combination resonance region. This dynamic behavior is due to the closeness of the second parametric frequency ($2\Omega_2 = 37.46\,\text{Hz}$) with respect to the first flexural–torsional mode. On the other hand, when the static load parameter increases ($\alpha = 0.5$), the relation between the parametrically excited

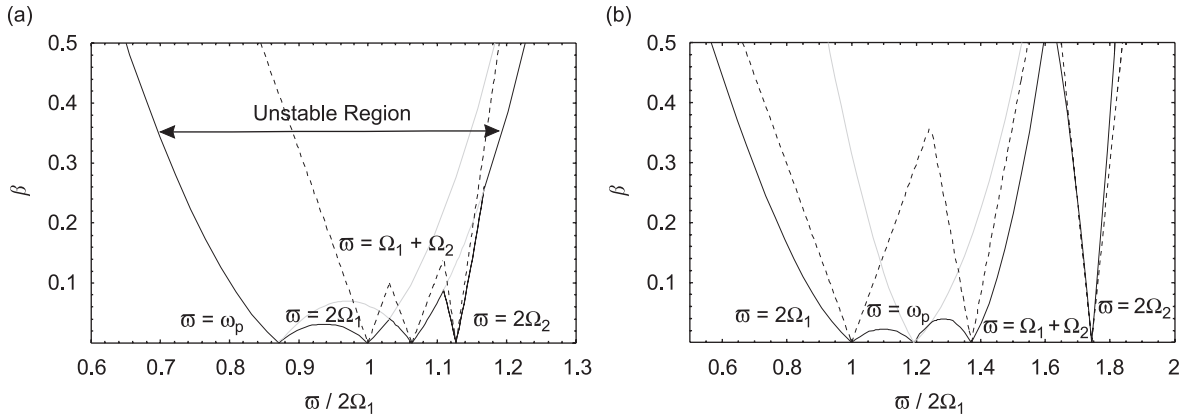

Fig. 16. Effect of static load parameter on unstable regions of a fixed-end beam, (———) present theory, (- - - - -) neglecting interaction with ω_p, (a) $\alpha = 0.5$ and (b) $\alpha = 0.1$.

frequencies also increases. In this case, the third instability region ($2\Omega_2 = 42.30$ Hz) moves away from the main unstable region ($2\Omega_1 = 24.26$ Hz). It is also observed that the influence of the interaction between the forced vibration and the parametrically excited vibrations enlarges the instability region to high frequency values (Fig. 16b). The larger unstable region is limited by the frequencies values corresponding to the main parametric and combination resonance.

The unstable boundaries obtained by disregarding this interaction are drawn in dashed lines and the difference between both formulations is higher for small static load parameter.

8.6. *Effect of approximations on the dynamic stability*

The purpose of this example is to show the effect of the degree of nonlinearity adopted in the displacement field Eq. (4) on the dynamic stability analysis. As it was pointed out in the introduction of this work a significant amount of research has been conducted in recent years toward the development of nonlinear theories of 3-D beams. However, many of these theories differ in the order of nonlinearity considered in their formulation. For example, second-order displacement field has been used in a formulation of finite element models for 3-D nonlinear analysis of beam structures [29–31]. This approximation presents several advantages because it simplifies the coupling between the displacement and rotations and so the tangent stiffness matrix (used for the nonlinear incremental-iterative analysis) can be simplified. Therefore, this tangent matrix can be decomposed into linear and second-order (nonlinear) stiffness matrices. In spite of these advantages, second-order formulation may produce the loss of some significant terms in the nonlinear strains and in the tangent stiffness matrix, thus some inaccurate approximations in the coupling between displacement, rotations and their derivates. The loss of these terms may lead to 'self-straining' caused by superimposed rigid-body motions [32,33].

In particular the second-order model was modeled approximating $\cos\phi$ and $\sin\phi$ by $(1-\phi^2/2)$ and ϕ, respectively, in Eq. (4) and conserving nonlinear terms up to second order. Therefore the displacement field yields:

$$
\begin{aligned}
u_x &= u_o - \theta_z\bar{y} - \theta_y\bar{z} + \phi\theta_z z - \phi\theta_y y + \omega\left[\theta - \tfrac{1}{2}(\theta'_y\theta_z - \theta_y\theta'_z)\right],\\
u_y &= v - \phi z + \tfrac{1}{2}(-\phi^2 y - \theta_z^2\bar{y} - \theta_z\theta_y\bar{z}),\\
u_z &= w + \phi y + \tfrac{1}{2}(-\phi^2 z - \theta_y^2\bar{z} - \theta_z\theta_y\bar{y}).
\end{aligned}
\tag{43}
$$

Then a second-order formulation Eq. (43), produces the loss of the terms underlined in Eq. (27). These terms correspond to the flexural–torsional coupling in the nonlinear strains. On the other hand, the unstable boundaries are also compared with the values obtained by means of the classical formulation, where the initial displacement due to static load and the influence of ω_p are neglected. In the classical model the regions of instability are obtained considering only initial stresses.

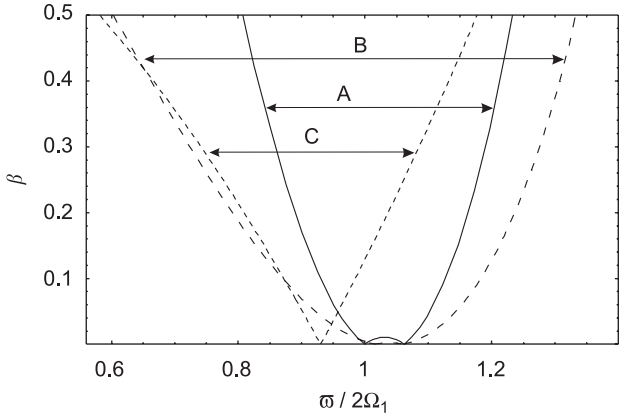

Fig. 17. Effects of approximations on regions of dynamic instability, (———) present model with width A, (— — —) 2° order formulation with width B, (- - - - -) classical or first-order approximation with width C, load applied to the top flange.

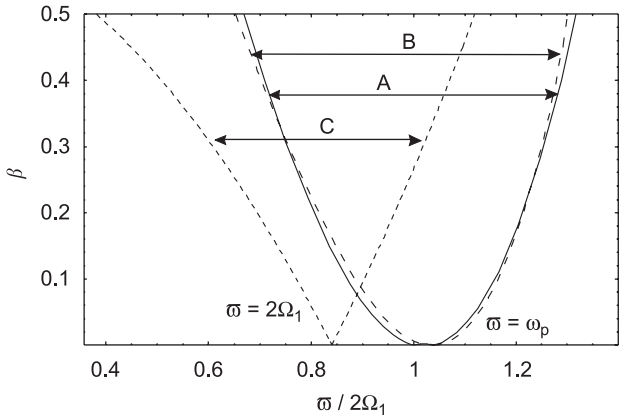

Fig. 18. Effects of approximations on regions of dynamic instability, (———) present model with width A, (— — —) 2° order formulation with width B, (- - - - -) classical or first-order approximation with width C, load applied at the shear center.

In this example a simply supported I-beam subjected to a transverse force P at the middle of the span is considered, for three load positions. The geometrical properties are $L = 6\,\text{m}$, $h = 0.6\,\text{m}$, $b = 0.6\,\text{m}$, $e = 0.03\,\text{m}$. The analyzed material is graphite-epoxy and the sequence lamination considered is $\{0/0/0/0\}$. Comparative results of regions of dynamic instability are shown in Figs. 17–19, for the load applied to the top flange, at the shear center and to the bottom flange, respectively. It is observed that the parametric frequencies values obtained with the second-order theory are higher than those obtained with the present formulation, for $\beta = 0$, while the natural frequency corresponding to the loading plane ω_p is the same for both models. Second-order approximation overestimates the stability behavior of composite beams as was mentioned by the authors in [20]. This effect is larger when the load is applied on the bottom face. With increasing the dynamic load parameter the unstable regions predicted by the second-order approximation are wider when the load is on the top flange and smaller when the load is applied on the bottom flange. Therefore, this approximation results, inadvertently, in a less critical behavior than in the case of the present model, when the load is applied on the bottom flange.

Significant differences are observed in the classical or first-order results due to geometrical nonlinear effects. The parametric frequencies calculated from the classical analysis are smaller compared with those calculated from the present nonlinear model, as was shown by the authors in [21]. Therefore, the unstable region moves toward the left originated by a decrease in the parametric frequency values. Besides, the unstable regions size is completely different to the ones obtained with the present model. This effect is due mainly to the coupling of the different types of motion, where their interaction is due to nonlinear effects.

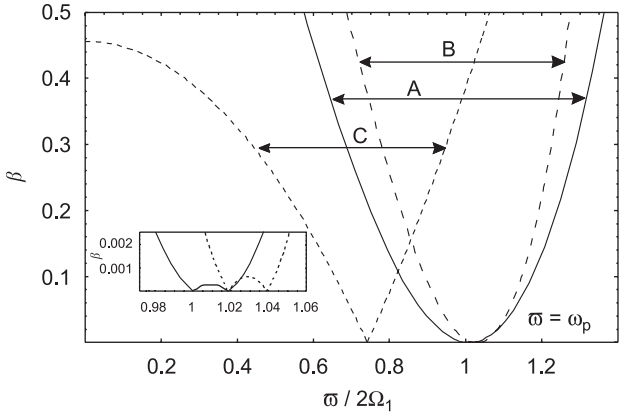

Fig. 19. Effects of approximations on regions of dynamic instability, (———) present model with width A, (— — —) 2° order formulation with width B, (-----) classical or first-order approximation with width C, load applied on the bottom flange.

9. Conclusions

In this paper, the influences of shear deformation and geometrically nonlinear coupling on the dynamic stability of thin-walled laminated composite beam are analyzed. A nonlinear beam theory is formulated in the context of large displacements and rotations, through the adoption of a shear-deformable displacement field (accounting for bending and warping shear). Regions of dynamic instability are studied for simply supported, cantilever and fixed-end composite beams subjected to transverse periodic loads. Unstable regions for simple and combination resonant frequencies are expressed in non-dimensional terms and determined by applying Hsu's procedure to the Mathieu equation. The influence of non-conventional effects is noted in the numerical results and can be summarized as follows:

1. The width of the instability regions increases with an increase in the static and dynamic loads.
2. The unstable regions sizes are influenced by the transverse shear effect, when this effect is ignored the boundaries of instability shift to the right. This behavior is originated by an increase in the parametric resonance frequency values and higher differences are observed when the beam length decreases.
3. The interaction between the forced vibration and the parametrically excited vibrations on the regions of dynamic instability is significant in some cases. This effect depends on the closeness of the frequency values, i.e. it depends on the stiffnesses ratio between the parametrically excited mode and the vertical mode corresponding to the loading plane.
4. This influence enlarges the unstable region because the unstable regions are composed by two regions, one of them lies near the parametric excited frequency and the other lies near the natural frequency corresponding to the loading plane, for small values of the dynamic load parameter.
5. In general, the discard of this interaction results, inadvertently, in a less critical behavior for the main parametric and combination unstable regions than in the case of its incorporation.
6. However, the second parametric unstable region is in general larger when the interaction is neglected, overpredicting the unstable behavior.
7. Second-order nonlinear approximation overestimates the stability behavior and the unstable regions size depends on the load height parameter. On the other hand, the parametrically excited frequencies obtained by a classical or first-order approximation are smaller in comparison with the ones obtained by the higher nonlinear present model.
8. The size of unstable regions depends on the load height parameter, for example the unstable regions are wider when the load is applied on the beam bottom flange.

Acknowledgment

The present study was sponsored by Secretaría de Ciencia y Tecnología, Universidad Tecnológica Nacional, and by CONICET.

Appendix A. Constitutive law

The constitutive law for a bisymmetric beam is defined in the following form:

$$\mathbf{f_g} = \mathbf{D}\boldsymbol{\chi}, \tag{A.1}$$

$$\mathbf{f_g} = \left\{ N \quad M_y \quad M_z \quad B \quad Q_y \quad Q_z \quad T_w \quad T_{sv} \quad B_1 \quad P_{yy} \quad P_{zz} \quad P_{yz} \right\}^{\mathrm{T}}, \tag{A.2}$$

$$\boldsymbol{\chi} = \left\{ ED_1 \quad ED_2 \quad ED_3 \quad ED_4 \quad ED_5 \quad ED_6 \quad ED_7 \quad ED_8 \quad ED_9 \quad ED_{10} \quad ED_{11} \quad ED_{12} \right\}^{\mathrm{T}}, \tag{A.3}$$

where $\mathbf{f_g}$ is the vector of generalized forces, $\boldsymbol{\chi}$ the vector of the generalized strains. The elements of the symmetric matrix $\mathbf{D}$ (12×12) are given by the following contour integrals, being null the matrix elements that are not indicated below:

$$
\begin{aligned}
K_{1,1} &= \int \bar{A}_{11}\,\mathrm{d}s, \\
K_{1,9} &= \int \bar{A}_{11}(Y^2+Z^2)\,\mathrm{d}s, \\
K_{1,10} &= \int \bar{A}_{11}\bar{Z}^2\,\mathrm{d}s, \\
K_{1,11} &= \int \bar{A}_{11}\bar{Y}^2\,\mathrm{d}s, \\
K_{1,12} &= \int \bar{A}_{11}\bar{Y}\bar{Z}\,\mathrm{d}s, \\
K_{2,2} &= \int \left(\bar{A}_{11}Z^2 + \bar{D}_{11}Y'^2\right)\mathrm{d}s, \\
K_{2,9} &= \int \left[\bar{A}_{11}\bar{Z}(Y^2+Z^2) - 2\bar{D}_{11}rY'\right]\mathrm{d}s, \\
K_{2,10} &= \int \left(\bar{A}_{11}\bar{Z}^3 + 2\bar{D}_{11}\bar{Z}Y'^2\right)\mathrm{d}s, \\
K_{2,11} &= \int \left(\bar{A}_{11}\bar{Y}^2\bar{Z} - 2\bar{D}_{11}\bar{Y}Y'Z'\right)\mathrm{d}s, \\
K_{2,12} &= \int \left[\bar{A}_{11}\bar{Y}\bar{Z}^2 + \bar{D}_{11}(\bar{Y}Y' - \bar{Z}Z')Y'\right]\mathrm{d}s, \\
K_{3,3} &= \int \left(\bar{A}_{11}Y^2 + \bar{D}_{11}Z'^2\right)\mathrm{d}s, \\
K_{3,9} &= \int \left[\bar{A}_{11}\bar{Y}(Y^2+Z^2) + 2\bar{D}_{11}rZ'\right]\mathrm{d}s, \\
K_{3,10} &= \int \left(\bar{A}_{11}\bar{Y}\bar{Z} - 2\bar{D}_{11}\bar{Z}Y'Z'\right)\mathrm{d}s, \\
K_{3,11} &= \int \left(\bar{A}_{11}\bar{Y}^3 + 2\bar{D}_{11}\bar{Y}Z'^2\right)\mathrm{d}s, \\
K_{3,12} &= \int \left[\bar{A}_{11}\bar{Y}^2\bar{Z} - \bar{D}_{11}(\bar{Y}Y' - \bar{Z}Z')Z'\right]\mathrm{d}s, \\
K_{4,4} &= \int \left(\bar{A}_{11}\omega_p^2 + \bar{D}_{11}l^2\right)\mathrm{d}s, \\
K_{4,9} &= \int \left[\bar{A}_{11}\omega_p(Y^2+Z^2) + 2\bar{D}_{11}rl\right]\mathrm{d}s, \\
K_{4,10} &= \int \left(\bar{A}_{11}\omega_p\bar{Z}^2 - 2\bar{D}_{11}\bar{Z}Y'l\right)\mathrm{d}s, \\
K_{4,11} &= \int \left(\bar{A}_{11}\omega_p\bar{Y} + 2\bar{D}_{11}\bar{Y}Z'l\right)\mathrm{d}s, \\
K_{4,12} &= \int \left[\bar{A}_{11}\bar{Y}\omega_p\bar{Z} - \bar{D}_{11}(\bar{Y}Y' - \bar{Z}Z')l\right]\mathrm{d}s, \\
K_{5,5} &= \int \left(\bar{A}_{55}Z'^2 + \bar{A}_{66}Y'^2\right)\mathrm{d}s, \\
K_{5,6} &= \int (\bar{A}_{66} - \bar{A}_{55})Z'Y'\,\mathrm{d}s, \\
K_{5,7} &= \int \left[\bar{A}_{66}Y'(r-\psi) - \bar{A}_{55}Z'l\right]\mathrm{d}s, \\
K_{5,8} &= \int \bar{A}_{66}\psi Y'\,\mathrm{d}s, \\
K_{6,6} &= \int \left(\bar{A}_{55}Y'^2 + \bar{A}_{66}Z'^2\right)\mathrm{d}s, \\
K_{6,7} &= \int \left[\bar{A}_{66}Z'(r-\psi) + \bar{A}_{55}Y'l\right]\mathrm{d}s, \\
K_{6,8} &= \int \bar{A}_{66}\psi Z'\,\mathrm{d}s, \\
K_{7,7} &= \int \left[\bar{A}_{66}(r-\psi)^2 + \bar{A}_{55}l^2\right]\mathrm{d}s, \\
K_{7,8} &= \int \bar{A}_{66}\psi(r-\psi)\,\mathrm{d}s, \\
K_{8,8} &= \int (\bar{A}_{66}\psi^2 + 4\bar{D}_{66})\,\mathrm{d}s, \\
K_{9,9} &= \int \left[\bar{A}_{11}(Y^2+Z^2)^2 + 4\bar{D}_{11}r^2\right]\mathrm{d}s, \\
K_{9,10} &= \int \left[\bar{A}_{11}(Y^2+Z^2)\bar{Z}^2 - 4\bar{D}_{11}\bar{Z}Y'r\right]\mathrm{d}s, \\
K_{9,11} &= \int \left[\bar{A}_{11}(Y^2+Z^2)\bar{Y}^2 + 4\bar{D}_{11}\bar{Y}Z'r\right]\mathrm{d}s, \\
K_{9,12} &= \int \left[\bar{A}_{11}(Y^2+Z^2)\bar{Y}\bar{Z} - 2\bar{D}_{11}(\bar{Y}Y' - \bar{Z}Z')r\right]\mathrm{d}s, \\
K_{10,10} &= \int \left(\bar{A}_{11}\bar{Z}^4 + 4\bar{D}_{11}\bar{Z}^2Y'^2\right)\mathrm{d}s, \\
K_{10,11} &= \int \left(\bar{A}_{11}\bar{Z}^2\bar{Y}^2 - 4\bar{D}_{11}\bar{Z}Y'\bar{Y}Z'\right)\mathrm{d}s, \\
K_{10,12} &= \int \left[\bar{A}_{11}\bar{Z}^3\bar{Y} + 2\bar{D}_{11}(\bar{Y}Y' - \bar{Z}Z')\bar{Z}Y'\right]\mathrm{d}s, \\
K_{11,11} &= \int \left(\bar{A}_{11}\bar{Y}^4 - 4\bar{D}_{11}\bar{Y}^2Z'^2\right)\mathrm{d}s, \\
K_{10,12} &= \int \left[\bar{A}_{11}\bar{Y}^3\bar{Z} - 2\bar{D}_{11}\left(\bar{Y}Y' - \bar{Z}Z'\right)\bar{Y}Z'\right]\mathrm{d}s, \\
K_{12,12} &= \int \left[\bar{A}_{11}\bar{Z}^2\bar{Y}^2 + \bar{D}_{11}(\bar{Y}Y' - \bar{Z}Z')^2\right]\mathrm{d}s,
\end{aligned}
\tag{A.4}
$$

where

$$Y' = \frac{\mathrm{d}Y}{\mathrm{d}s}, \quad Z' = \frac{\mathrm{d}Z}{\mathrm{d}s}. \tag{A.5}$$

References

[1] R.M. Evan-Iwanowski, On the parametric response of structures, *Applied Mechanics Review* 18 (1965) 699–702.
[2] A.H. Nayfeh, D.T. Mook, *Nonlinear Oscillations*, Wiley, New York, 1979.
[3] V.V. Bolotin, *The Dynamic Stability of Elastic Systems*, Holden-Day, San Francisco, 1964.
[4] I.I. Gol'denblat, *Contemporary Problems of Vibrations and Stability of Engineering Structures*, Stroiizdat, Moscow, 1947.
[5] W.K. Tso, Parametric torsional stability of a bar under axial excitation, *Journal of Applied Mechanics* 35 (1968) 13–19.
[6] E. Mettler, Dynamic buckling, in: W. Flugge (Ed.), *Handbook of Engineering Mechanics*, McGraw-Hill, New York, 1962.
[7] A.A. Ghobarah, W.K. Tso, Parametric stability of thin-walled beams of open section, *Journal of Applied Mechanics, Transactions of ASME* 39 SER E (1) (1972) 201–206.
[8] V.V. Bolotin, On the parametric excitation of transverse vibrations, *Collection of Papers: Transverse Vibrations and Critical Velocities* 2 (1953) 5–44.
[9] C.H. Popelar, Dynamic stability of the flexural vibrations of a thin-walled beam, *International Journal of Solids and Structures* 5 (1969) 549–557.
[10] C.H. Popelar, Dynamic stability of thin-walled column, *Journal of Engineering, Mechanics Division, Proceedings of the American Society of Civil Engineers* 98 (1972) 657–677.
[11] S.A. Hasan, A.D.S. Barr, Non-linear and parametric vibration of thin-walled beams of equal angle-section, *Journal of Sound and Vibration* 31 (1) (1974) 25–47.
[12] T.W. Kim, J.H. Kim, Parametric instability of a cross-ply laminated beam with viscoelastic properties under a periodic force, *Composite Structures* 51 (3) (2001) 205–209.
[13] C.Y. Lin, L.W. Chen, Dynamic stability of rotating composite beams with a viscoelastic core, *Composite Structures* 58 (2) (2002) 185–194.
[14] A. Sapkás, L.P. Kollár, Lateral–torsional buckling of composite beams, *International Journal of Solids and Structures* 39 (11) (2002) 2939–2963.
[15] V.H. Cortínez, M.T. Piovan, Vibration and buckling of composite thin walled beams with shear deformability, *Journal of Sound and Vibration* 258 (4) (2002) 701–723.
[16] V.H. Cortínez, M.T. Piovan, Stability of composite thin-walled beams with shear deformability, *Computers & Structures* 84 (15–16) (2006) 978–990.
[17] T.A. Morey, E. Johnson, C.K. Shield, A simple beam theory for the buckling on symmetric composite beams including interaction of in-plane stresses, *Composites Science and Technology* 58 (8) (1998) 1321–1333.
[18] S.P. Machado, V.H. Cortínez, Non-linear model for stability of thin walled composite beams with shear deformation, *Thin-Walled Structures* 43 (10) (2005) 1615–1645.
[19] S.P. Machado, C.P. Filipich, V.H. Cortínez, Parametric vibration of thin-walled composite beams with shear deformation, *Journal of Sound and Vibration* 305 (4–5) (2007) 563–581.
[20] S.P. Machado, V.H. Cortínez, Lateral buckling of thin walled composite bisymmetric beams with prebuckling and shear deformation, *Engineering Structures* 27 (8) (2005) 1185–1196.
[21] S.P. Machado, V.H. Cortínez, Free vibration of thin-walled composite beams with static initial stresses and deformations, *Engineering Structures* 29 (3) (2007) 372–382.
[22] C. Hsu, On the parametric excitation of a dynamic system having multiple degrees of freedom, *Journal of Applied Mechanics* 30 (1963) 367–372.
[23] E.J. Barbero, *Introduction to Composite Material Design*, Taylor & Francis, London, 1999.
[24] J.N. Reddy, *Mechanics of Laminated Composite Plates and Shells: Theory and Analysis*, second ed., CRC Press, Boca Raton, FL, 2004.
[25] J.H. Argyris, An excursion into large rotations, *Computer Methods in Applied Mechanics and Engineering* 32 (1–3) (1981) 85–155.
[26] S. Krenk, O. Gunneskov, Statics of thin-walled pre-twisted beams, *International Journal of Numerical Methods in Engineering* 17 (9) (1981) 1407–1426.
[27] K. Washizu, *Variational Methods in Elasticity and Plasticity*, Pergamon Press, Oxford, 1968.
[28] P. Hagedorn, L.P. Koval, On the parametric stability of a Timoshenko beam subjected to a periodic axial load, *Ingenieur Archiv* 40 (3) (1971) 211–220.
[29] A. Hasegawa, K.K. Liyanage, F. Nishino, Spatial instability and nonlinear finite displacement analysis of thin walled members and frames, *Journal of the Faculty of Engineering, University of Tokyo, Series B* 38 (4) (1986) 19–78.
[30] S. Kitipornchai, S.L. Chan, Stability and nonlinear finite element analysis, in: J.W. Bull (Ed.), *Finite Element Applications to Thin-Walled Structures*, Elsevier Applied Science, London, 1990, pp. 89–130.
[31] T.M. Roberts, Instability, geometric non-linearity and collapse of thin walled beams, in: R. Narayanan (Ed.), *Beams and Beam-Columns-Stability and Strength*, Applied Science Publishers, London, UK, 1983, pp. 135–160.
[32] Y.L. Pi, M.A. Bradford, Effects of approximations in analysis of beams of open thin walled cross-section—part II: 3-D non-linear behaviour, *International Journal of Numerical Methods in Engineering* 51 (7) (2001) 773–790.
[33] J.C. Simo, L. Vu-Quoc, The role of non-linear theory in transient dynamic analysis of flexible structures, *Journal of Sound and Vibration* 119 (3) (1987) 487–508.